THE JOURNAL OF PHYSICAL CHEMISTRY C
A JOURNAL OF THE AMERICAN CHEMICAL SOCIETY

pubs.acs.org/JPCC
Perspective

Photocatalytic Processes at the Nanoscale: From Metals to Semiconductors

Published as part of The Journal of Physical Chemistry C special issue "Naomi Halas and Peter Nordlander Festschrift".

Swati J. Patil, Charles L. Mitchell, and Dmitry Kurouski*

Cite This: J. Phys. Chem. C 2025, 129, 7154−7164

ABSTRACT: Light can interact with metallic nanostructures, generating localized surface plasmon resonances (LSPRs) that enhance Raman scattering from molecules located close to nanostructure surfaces, a phenomenon known as surface-enhanced Raman scattering (SERS). LSPRs decay producing hot carriers, highly energetic species responsible for chemical transformations that can be monitored using SERS or its nanoscale analogue, tip-enhanced Raman spectroscopy (TERS). During the past decade both SERS and TERS provided a wealth of information about the physics and chemistry of hot carrier-driven reactions on mono- and bimetallic nanostructures. Recently, the same photochemical reactions have been observed on two-dimensional transition metal dichalcogenides (2D TMDs), a novel class of semiconductors. This discovery opened new questions about the underlying physics of photocatalysis that remain unresolved. The review delves into the physics and chemistry of photocatalysis on 2D TMDs, building on previous studies **of photocatalytic reactions with mono- and bimetallic nanostructures.** It also provides a critical discussion of the role of **nanoscale imaging in investigating photocatalytic processes**, emphasizing the valuable insights **such analyses can provide to synthetic chemists, material scientists, physicists, and biologists**.

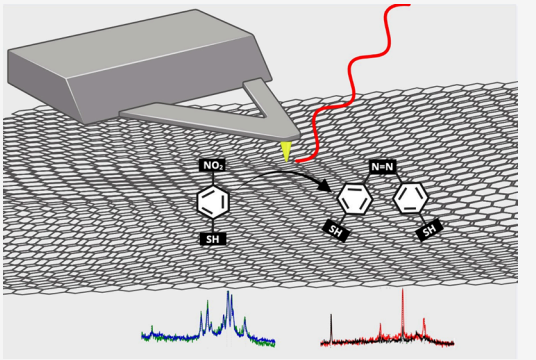

INTRODUCTION

Light can interact with metallic nanomaterials producing localized surface plasmon resonances (LSPRs) on the metal surfaces.[1−6] From a physical perspective, LSPRs are coherent oscillation of conductive electrons.[7−9] Their energies are determined by the nature of the metal and size and surrounding of the nanostructures.[7,10] Consequently, changes in these parameters would alter the absorption properties of the nanostructures.[11−14] This physical phenomenon is broadly used for sensing of gases and various analytes in solutions.[15−17]

LSPRs are also the underlying physical cause of surface enhancement of Raman scattering.[2,18−21] First observed by Fleishman on roughened silver surfaces, this effect was explained by Van Duyne in 1974.[22] Since then, surface-enhanced Raman spectroscopy (SERS) is broadly used in various scientific areas ranging from material science and forensics to biology and art conservation science.[2,18−21] Metallic nanostructures can be formed on the surface of the scanning probes used in atomic force microscopy (AFM) or electrochemically etched at the apexes of metallic wires.[23,24] In this case, illumination of such metallized or metallic scanning probes by light generates LSPRs at the probe apex.[25,26] If rastered across the sample surface, metallized AFM probes enable an acquisition of its chemical map with nanometer spatial resolution.[27−31] This advantage made TERS highly useful for the nanoscale structural analysis of biological[32−35] and polymer[36−38] samples, as well as electrochemical[25,39−41] catalytic[42−45] processes at solid−liquid and solid−gas interfaces.

In TERS, catalysis is defined as analyzing and enhancing catalytic phenomena on the nanoscale with a high degree of spatial precision. It extends the capabilities of traditional scanning microscopy and offers real time probing of surface reactions, their intermediates, and active sites on catalysts.[46] TERS has great value for investigating plasmon-driven catalysis, providing detailed molecular information on the products of reactions. It is used to study the behavior of catalysts with reactants, the effect of surface plasmons on the rate of reaction, and the performance of catalysts in various operating conditions. As many monofunctional catalysts have been studied and shown to lose efficiency over time,[47] TERS has become an essential tool

Received: February 17, 2025
Revised: March 27, 2025
Accepted: March 27, 2025
Published: April 7, 2025

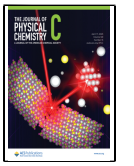

https://doi.org/10.1021/acs.jpcc.5c01084
J. Phys. Chem. C 2025, 129, 7154−7164

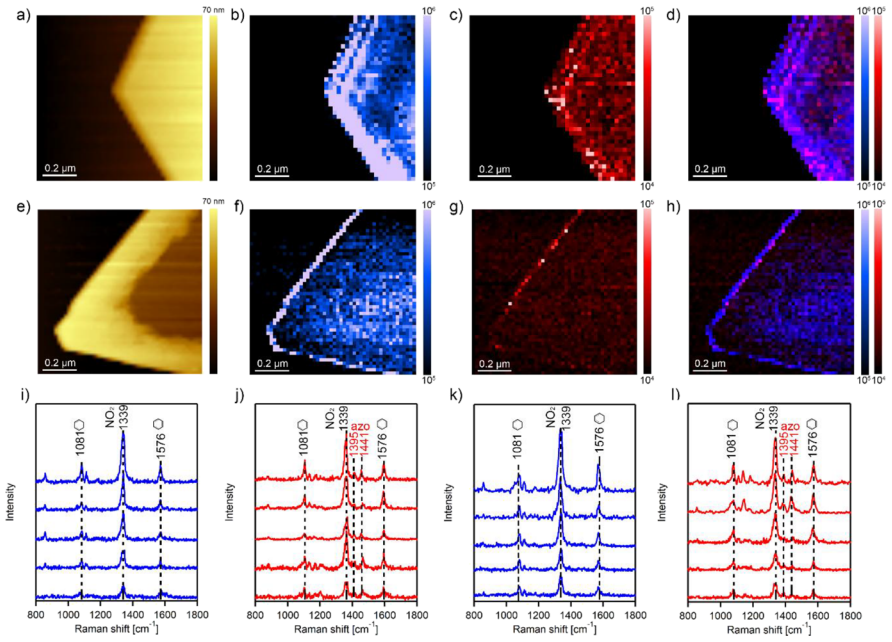

Figure 1. (a) AFM images of AuMPs and (e) WAuMPs. TERS images of (b-d) AuMPs and (f-h) WAuMPs (20 nm per pixel). Intensity of 1339 cm^{-1} band (NO_2) of 4-NBT is shown in blue, intensities of 1397 and 1441 cm^{-1} (azo) of DMAB is shown in red. (i-l) Typical TERS spectra extracted from chemical maps on (b and f) showing presence of 4-NBT (blue). Randomly picked TERS spectra from chemical maps shown in (c and g) demonstrate the presence of DMAB (red). Reprinted with permission from ref 67. Copyright (2021) American Chemical Society.[76]

for investigating plasmon-driven surface processes, especially in photocatalysis, where it helps reveal detailed reaction mechanisms.[46,48] This knowledge is crucial for developing more efficient photocatalysts for a wider range of applications including energy conversion and environmental remediation.

UNDERLYING PHYSICS OF PHOTOCATALYSIS ON METALS AND SEMICONDUCTORS

LSPRs have a relatively short lifetime quickly decaying via radiative and nonradiative pathways.[49−51] Upon radiative decay, energy is dissipated through the elastic scattering of incident photons. However, in the case of nonradiative decay, LSPRs produce hot carriers.[52,53] These highly energetic species persist only a few tens of femtoseconds further decaying by electron−electron or electron−phonon scattering.[52,53] Hot carriers can be directly or indirectly injected into electronic states of molecules that present close to the metal surfaces.[54,55] This triggers chemical transformation, which in turn, can be observed using the SERS effect.[54,55] Several research groups proposed alternative mechanisms of photocatalysis on metallic surface.[56−59] Hot electrons and holes have unequal dissipation rates on metallic surfaces.[57,58] This asymmetry in dissipation rates results in the formation of a "steady-state charge" or the "electrostatic potential" on the nanostructure surfaces.[57,58] The Jain group provided an excellent set of experimental and theoretical evidence of why the steady-state charge should be considered as a catalytic force of chemical reactions.[60] Thus, electrostatic potential rather than hot carriers themselves can be the underlying cause of chemical reactions observed on metallic nanomaterials.[57,58] Our group showed that the magnitude of the electrostatic potential on mono- and bimetallic nanostructures had a direct correlation with the intensity of the light used for their illumination.[61,62] Furthermore, the intensity of the electrostatic potential could be uniquely altered by doping gold (Au) nanostructure with catalytic metals, such as platinum (Pt) and palladium (Pd).[63,64] Using TERS, we also showed that the magnitude of the electrostatic potential had a direct correlation with the yield of photochemical reactions on mono- and bimetallic nanostructures.[63] Thus, we demonstrated a clear relationship among light intensity, electrostatic potential, and catalytic reactivity.

Two-dimensional transitional metal dichalcogenides (2D TMDs) are a novel class of semiconductors that have unique optical, catalytic, and biological properties.[20−22,32−34,65,66] As a result, these nanomaterials attract a lot of interest as potential light sources,[26,27] optical modulators,[28] photodetectors,[29] field-effect transistors,[30] logic circuits,[31] sensors,[20−22,32−34] catalysts, and biostimulants. The Raschke group proposed that the observed catalytic reactivity of both MoS_2 and MoS_2@AuNPs is determined by dark excitons that have antiparallel spin configuration with generally forbidden radiative emission.[67−69] Additionally, the same group proposed a local probe technique to determine the intrinsic properties of the 2D heterostructure of graphene semiconductor (WSe_2).[70] Park and co-workers showed that coupling of plasmonic scanning probe with WS_2 resulted in a high yield of dark excitons, which in turn, can trigger chemical transformation.[67−69] Hasz et al. conducted a study on tip-enhanced photoluminescence spectroscopy, using atomic force-induced strain control to nanoimage dark excitons in WSe_2 and investigate their response to local strain.[71] The significance of TMD heterostructures (WS_2/MoS_2) for photodetectors was highlighted in work by Wang et al., fabricated photodetectors that showed an approximately 25-fold enhancement in infrared responsivity, studied through surface plasmon resonance.[72]

TERS Imaging of Photocatalytic Processes on Monometallic Nanostructure. The first experimental evidence of plasmon-driven photocatalysis was demonstrated in 2012 by Van Schrojenstein Lantman and co-workers.[73] In this experiment, the researchers utilized a silver (Ag) tip and Au microplate (AuMPs) coated with 4-nitrobenzenethiol (4-NBT). Once the tip was approached on the nanoplate surface and illuminated by light, 4-NBT dimerization into *p,p′*-dimercaptoazobisbenzene

https://doi.org/10.1021/acs.jpcc.5c01084
J. Phys. Chem. C 2025, 129, 7154−7164

(DMAB) was observed. This conclusion could be made by the appearance of 1397 and 1441 cm^{-1} vibrational bands in the acquired TERS spectra. Thus, it was found that TERS could be used to trigger and monitor photocatalytic processes. It was also found that the DMAB yield was wavelength dependent. Specifically, a substantially lower yield of DMAB was observed if 633 nm laser light was used to illuminate the probe compared to 532 nm excitation.

Kurouski group used TERS to examine photocatalytic properties of different surface sites on AuMPs and their nanoscale analogs (gold nanoplates (AuNPs)).[64,74,75] Li and co-workers found that edges and corners of these AuNPs and AuMPs had much greater reactivity in 4-NBT to DMAB conversion compared to the central parts of nano- and microstructures, Figure 1a–d.[74]

Li and Kurouski proposed that reactivity of the edges and corners was determined by the magnitude of the rectified electric field at these surface sites.[74] To test this hypothesis, researchers used 4-mercaptobenzonitrile (4-MBN) as a molecular reporter.[62] A frequency of the nitrile vibration is highly sensitive to the intensity of a rectified electric field.[77,78] Consequently, its shift can be used to quantify the intensity of the rectified electric field on the surface of the nanostructures.[77,79] The reported findings showed that corners and edges of gold nanostructures had stronger, on average, magnitude of the rectified electric field compared the central parts of the nanostructures.[62]

Using TERS, the El-Khoury group investigated photocatalytic properties of Ag nanowires (AgNWs) and Ag nanoparticles (AgNPs).[80,81] It was found that edges and corners of these Ag nanostructures showed stronger intensities of the rectified electric field compared to their flat terraces.[82,83] Thus, one can conclude that differences between the intensity of the rectified electric field at the edges, corners, and central parts of the nanostructures and, consequently, the reactivity of such surface sites are similar for Ag and Au nanostructures.

Li and co-workers used TERS to compared the reactivity of Ag and Au nanostructures.[84] It was found that AgNPs are far more reactive in 4-NBT to DMAB conversion compared to AuNPs, as shown in Figure 2. These findings indicate that TERS can be used not only for the nanoscale analysis of photocatalytic reactivity but also for the direct quantification of the yield of chemical reactions on the metallic nanomaterials.

The Zenobi group found that the density of molecular species on the surfaces of metallic nanostructures plays an important role in photocatalytic transformations.[37] It was found that surface sites with a high density of 4-NBT had significantly greater reactivity compared to surface sites with a low density of 4-NBT. Independently, the Ren group found that, on AgNPs, 4-aminothiophenol (4-ATP) was oriented at the angle relative to the metallic surfaces.[85] This molecular orientation enabled instantaneous photocatalytic dimerization of 4-ATP into DMAB. At the same time, strongly vertical orientation of this molecular analyte on Ag(111) inhibited dimerization of 4-ATP into DMAB. The researchers explained low reactivity of 4-ATP on Ag(111) by π-interactions of the molecular analytes.[37,76,85] Similar conclusions were made by Wang and Kurouski upon the TERS-based analysis of walled microplates. Such nanostructures formed from AuMPs upon heating to 400 °C for 30–120 min, which causes migration of Au atoms from the edges of the nanostructures toward their centers.[86] It was found that wall-AuMPs produced 16 times lower yields of DMAB compared to the AuMPs that had Au(111) on their surfaces. Based on these

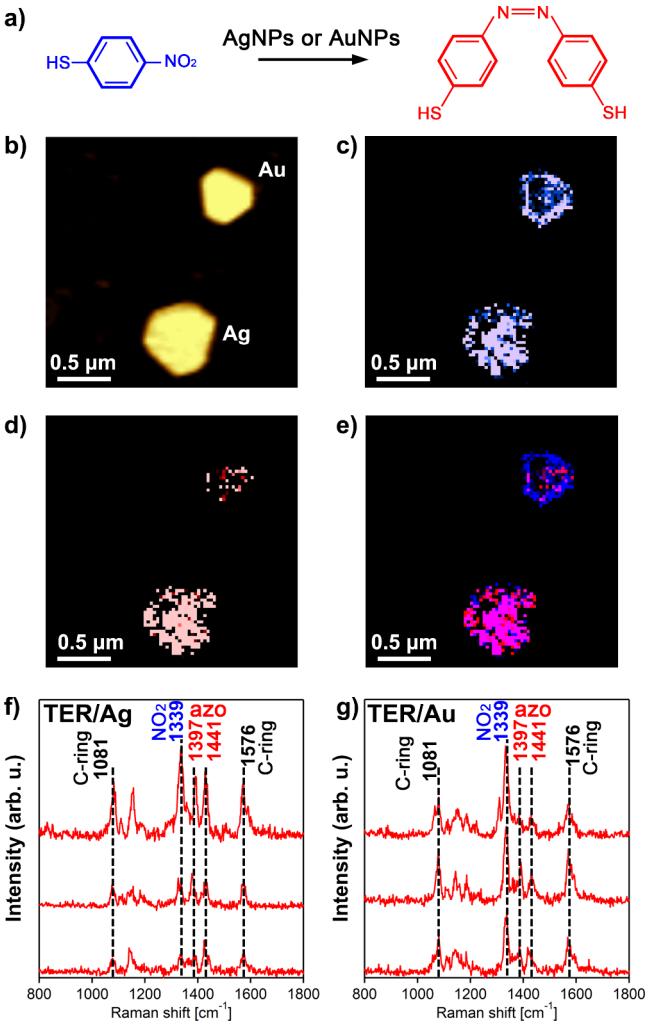

Figure 2. Plasmon-driven transformations of 4-NBT into DMAB on AuNPs and AgNPs. (a) Reaction scheme of 4-NBT reduction to DMAB. (b) Corresponding AFM image of AuNPs and AgNPs. TERS maps of (c) 4-NBT and (d) DMAB, as well as the overlapping TERS image of 4-NBT and DMAB (e) (10 nm per pixel). Intensity of 1339 cm^{-1} band (NO_2 vibration) of 4-NBT is shown in blue; intensities of 1397 and 1441 cm^{-1} (azo vibration) of DMAB are shown in red. Typical TERS spectra extracted from chemical maps on (f) AgNPs and (g) AuNPs showing the presence of 4-NBT (blue) and DMAB (red). Scale bar is 500 nm in each map. Reprinted with permission from ref 84. Copyright 2023 American Chemical Society.

results, the researchers concluded that the reactivity of the nanostructures directly depended on the crystal facets on their surfaces. Using 3D-TERS and transmission electron microscopy (TEM), Wang and Kurouski further investigated the relationship between metal crystal facets and catalytic reactivity of AuMPs.[87] The researchers discovered that Au(111) at the top of AuMPs yielded a much higher amount of DMAB compared to Au(100) and Au(110) facets located on the sides of AuMPs.[87] It should be noted that Rossi and coauthors found that (100) facets demonstrated higher reactivity in plasmon-driven reactions compared to (111) facets.[88] These results indicate additional studies are required to fully understand the relationship between the yield of the plasmon-driven reaction on monometallic nanostructures and their crystal facet structures.

https://doi.org/10.1021/acs.jpcc.5c01084
J. Phys. Chem. C 2025, 129, 7154–7164

The Kurouski group also examined catalytic reactivity of nanomaterials made out of nontraditional plasmonic metals such as magnesium (Mg) and copper (Cu).[89,90] It was found that Cu nanowires and nanocubes (CuNWs and CuNCs) exhibited great catalytic reactivity in the light-driven transformation of 4-NBT to DMAB, as shown in Figure 3. Furthermore, TERS revealed that edges and corners of these nanostructures were more reactive compared to their central parts. It was also discovered that CuNWs and CuNCs could oxidize 4-mercaptophenyl-methanol (4-MPM) to 4-mercaptobenzoic acid (4-MBA).[89] Such chemical transformations were not evident on AuNPs that only formed thiophenol from 4-MBA exposed to their surfaces. It should be noted that the reverse reaction of the reduction of 4-MPM into 4-MBA was inhibited by the binding of 4-MBA to the Cu surface via the carboxyl group. Patil and co-workers found that MgNPs possess a thick layer of oxide (MgO) on their surfaces that presents plasmon-driven conversion of 4-NBT to DMAB.[90] However, this problem can be solved by coupling Au nanoparticles with MgNPs. Such nanoparticles exhibited excellent photocatalytic reduction of 4-NBT to DMAB that were not observed on MgNPs.[90]

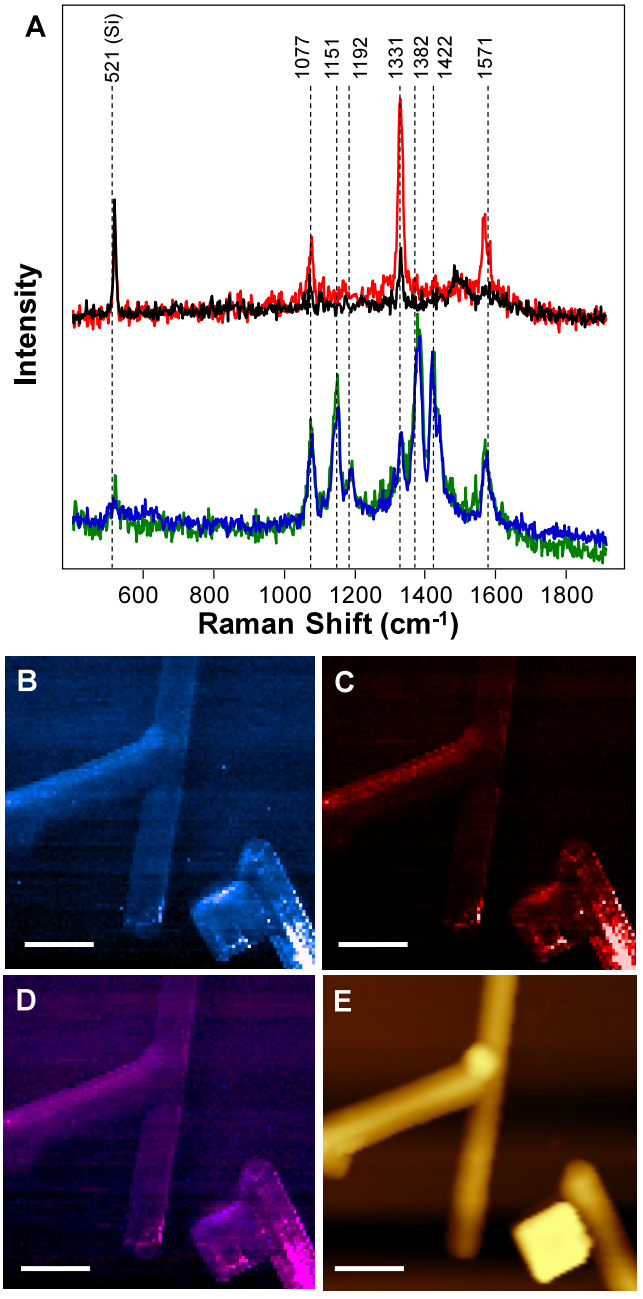

Figure 3. TERS on CuNWs and CuNCs. (A) TERS spectra collected from CuNWs and CuNCs (red) and Si wafer (black) as well as spectra of DMAB formed on CuNWs (blue) and CuNCs (green). (B) TERS image of 4-NBT (1331 cm^{-1}). (C) TERS image of DMAB (1382 cm^{-1}/1422 cm^{-1}). (D) Overlapped 4-NBT and DMAB images with the corresponding AFM image of the analyzed CuNWs and CuNCs (E). Scale bar: 500 nm. Reprinted with permission from ref 89. Copyright 2021 American Chemical Society.

Photocatalysis on Bimetallic Nanostructures. Bimetallic nanostructures have the potential to produce synergistic effects that enhance properties such as catalytic activity, stability, and selectivity. They are particularly valuable in fields such as catalysis, where enhanced performance is required. Bimetallic nanostructures not only demonstrate superior yield of photocatalytic reactions compared to their monometallic counterparts[90] but also allow for broadening the spectrum of chemical transformation that can be catalyzed by such nanostructures.[91] The latter is achieved by coupling catalytic metals with plasmonic nanostructures.[14,91] In this case, plasmonic metals harvest light and produce LSPRs that are passed on the catalytic metals that, in turn, trigger chemical reactions.[91] Noble and catalytic metal nanostructures can be localized in the close proximity to each other.[92,93] This catalytic concept is known as "antenna-reactor" reactor. Alternatively, catalytic metal can form a mono- or submonolayer on the surface of plasmonic nanostructures.[76] These nanomaterials are known as "sandwich" nanostructures.[91] Finally, atoms of plasmonic and catalytic nanostructures can be mixed within one nanostructure, forming an alloy.[32,33] In the case of "sandwich" and alloy nanostructures, the interplay between plasmonic and catalytic metals determines the reactivity of the catalysts. Using TERS, Li and Kurouski group examined photocatalytic properties of sandwich-like and alloy gold−palladium (Au@Pd) bimetallic nanostructures.[76] It was found that both nanostructures were able to reduce 4-NBT to both DMAB and 4-ATP. The formation of the latter product was evident only on Au@Pd and was not observed on AuNPs. The researchers demonstrated that sandwich-like Au@PdNPs yielded ∼65% DMAB and only ∼6% 4-ATP. At the same time, alloy Au@PdNPs produced ∼47 and ∼17%.[76] Thus, alloy-type bimetallic nanostructures yieldeda greater amount of 4-ATP compared to their sandwich-like analogs.

The Ren group utilized phenyl isocyanide (PIC) as a molecular reporter to map nanoscale reactivity of submonolayer of Pd on Au surface.[94] The researchers showed that TERS spectra acquired at Pd edges had C≡N vibration of PIC red-shifted on 60 cm^{-1} compared to the spectra collected from Pd atoms present at Au islands. These results demonstrated that molecules located at Pd edges had higher reactivity compared to Pd atoms present in terraces. A similar approach was used by the Ren group to probe electronic properties of Pt nanoislands on the surface of Au film.[95] In TERS spectra collected from lower-coordinated Pt sites, the researchers observed the C≡N vibration of 4-chlorophenyl isocyanide to be blue-shifted. Expanding upon these findings, the Ren and Zenobi groups examined nanoscale catalytic properties Pd submonolayer present on Au (111) surface.[96] It was found that catalytic hydrogenation of chloronitrobenzenethiol occurred beyond the location of Pd sites and was observed as far as 20 nm from the

https://doi.org/10.1021/acs.jpcc.5c01084
J. Phys. Chem. C 2025, 129, 7154−7164

bimetallic Pd/Au boundary. These results indicate that the interplay between plasmonic and catalytic metals at the nanoscale is far more complex than was previously expected.

Using TERS, Li and Kurouski investigated catalytic properties of gold−platinum (Au@Pt) and gold−palladium (Au@Pd) "sandwich-like" bimetallic nanoplates.[64] It was found that Au@PtNPs could be used to oxidize 4-MPM to 4-MBA, whereas the reversed reduction of 4-MBA to 4-MPM was evident only for Au@PdNPs, Figure 4.[64] However, in the absence of the catalytic

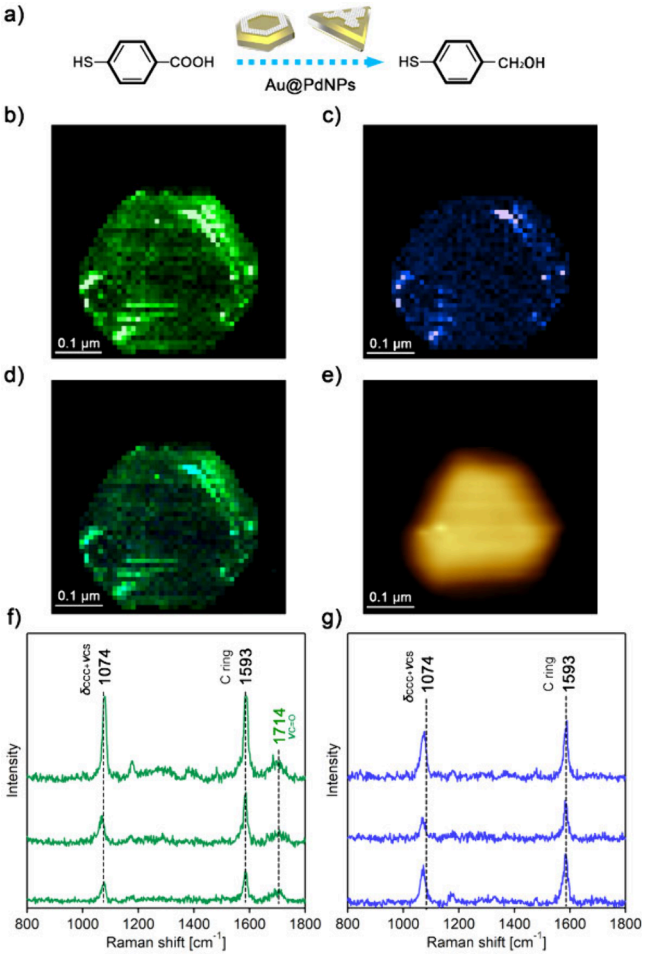

Figure 4. Plasmon-driven reduction of 4-MBA to 4-MPM on Au@PdNPs. (a) Schematic illustration of MBA reduction to MPM by Au@PdNPs; (b, c) TERS images of Au@PdNPs (10 nm per pixel). Intensity of intensities of 1570−1750 cm^{-1} containing C ring vibration and C═O vibration of 4-MBA is shown in green; the 1593 cm^{-1} band (C ring vibration) of MPM without showing a C═O vibration band (1714 cm^{-1}) is shown in blue. (d) Overlapping TERS images of 4-MPM and 4-MBA. (e) In situ AFM image of Au@PdNPs during TERS imaging. (f, g) Typical TERS spectra extracted from chemical maps on Au@PdNPs (panels a and b) showing the presence of 4-MPM (blue) and 4-MBA (green). Reprinted with permission from ref 64. Copyright 2021 American Chemical Society.

metals, the nanostructures were able to decarboxylate both 4-MBA and 4-MPM, producing thiophenol. These findings demonstrated that Pt determines unique oxidation, whereas Pd determines unique reduction properties of bimetallic nanostructures.

Recently, Patil and Kurouski reported TERS-based analysis of dimerization of aromatic halides on Ni-doped Au nanostructures.[97] It was found that such nanostructures enabled the highly efficient dimerization of aromatic halides into biphenyl. Furthermore, the greatest yield of biphenyl was observed on the Ni nanoislands present on the surface of Ni@Au nanostructures, Figure 5. However, such nanostructure-specific reactivity was not observed for copper−ruthenium nanoplates (Cu@RuNPs). Patil and Kurouski observed nearly uniform reactivity of Cu@RuNPs in dimerization of 4-NBT into DMAB.[98] It should be noted that Cu@RuNPs yielded nearly a 5 times greater amount of DMAB compared to their monometallic analogs (CuNPs).[98]

Photocatalysis on Semiconductors. 2D TMDs have unique properties, and TERS' nanoscale analysis makes it a powerful tool for photocatalysis research. It provides insights into fundamental processes and helps to optimize next-generation photocatalytic materials. The number of layers affects their properties, with monolayer TMDs offering enhanced electronic, catalytic, and optical traits.[99,100] These advantages make them ideal for optoelectronic applications and boost catalytic activity, which is essential for photocatalysis. Lambin and co-workers discovered that monolayer molybdenum disulfide (MoS_2) flakes could catalyze photocatalytic reduction of 4-nitrothiophenol (NTP) to *p,p′*-dimercaptoazobisbenzene (DMAB) and aminothiophenol (ATP),[101] a chemical reaction that was previously evident only for plasmonic metals.[102] Additionally, other studies showed that the nitro group (4-nitrobenzenediazonium (4-NBD) tetrafluoroborate salt) was reduced to a dimer through electron transfer from MoS_2, contributing to the doping process that alters the electronic band gap and excitonic properties of MoS_2.[103] The behavior of monolayer to few-layer MoS_2, showing significant changes in the intensities of the A_1g and E_2g modes, along with blue and red shifts, as demonstrated by Farhat et al., revealed that the MoS_2 monolayer exhibited enhanced optical absorption and greater electron−hole pair generation, as evidenced by the tip-enhanced photoluminescence (PL) emission.[104]

Using TERS and its infrared analogue, atomic force microscopy infrared (AFM-IR) spectroscopy, our group demonstrated that MoS_2 could catalyze dehalogenation of 4-bromothiophenol (4-BTP) producing thiophenol as well as dimerize 4-BTP into biphenyl. Patil and Kurouski also found that catalytic properties of single MoS_2 nanoflakes could be enhanced by doping gold nanoparticles onto the nanoflakes. The doping did not alter the amount of thiophenol produced by the nanostructures but increased the yield of biphenyl more than 3 times on MoS_2@AuNPs compared to MoS_2 nanoflakes. It should be noted that the same conclusions were made by independent analysis of the nanostructures using AFM-IR, which excludes the possibility of tip-based catalysis of 4-BTP to thiophenol or biphenyl conversion.

Recently, Patil and Kurouski used TERS to examine photocatalytic reduction of 4-NTP to DMAB on monolayer tungsten disulfide (WS_2) nanoplates and WS_2 coupled with palladium nanoparticles (WS_2@PdNPs), Figure 6.[65] It was found that both nanomaterials were able to catalyze the reduction of 4-NTP to DMAB. However, the yield of DMAB was substantially greater on WS_2@PdNPs compared to that on WS_2NPs. The researchers also found that an increase in the light intensity caused an increase in the reaction rate of 4-NTP to DMAB conversion on both WS_2 and WS_2@Pd nanoplates. The observed first-order kinetic relationship for DMAB formation on WS_2 nanoplates and WS_2@PdNPs hybrids indicated that their surfaces could possess both covalently anchored 4-NBT and an

https://doi.org/10.1021/acs.jpcc.5c01084
J. Phys. Chem. C 2025, 129, 7154−7164

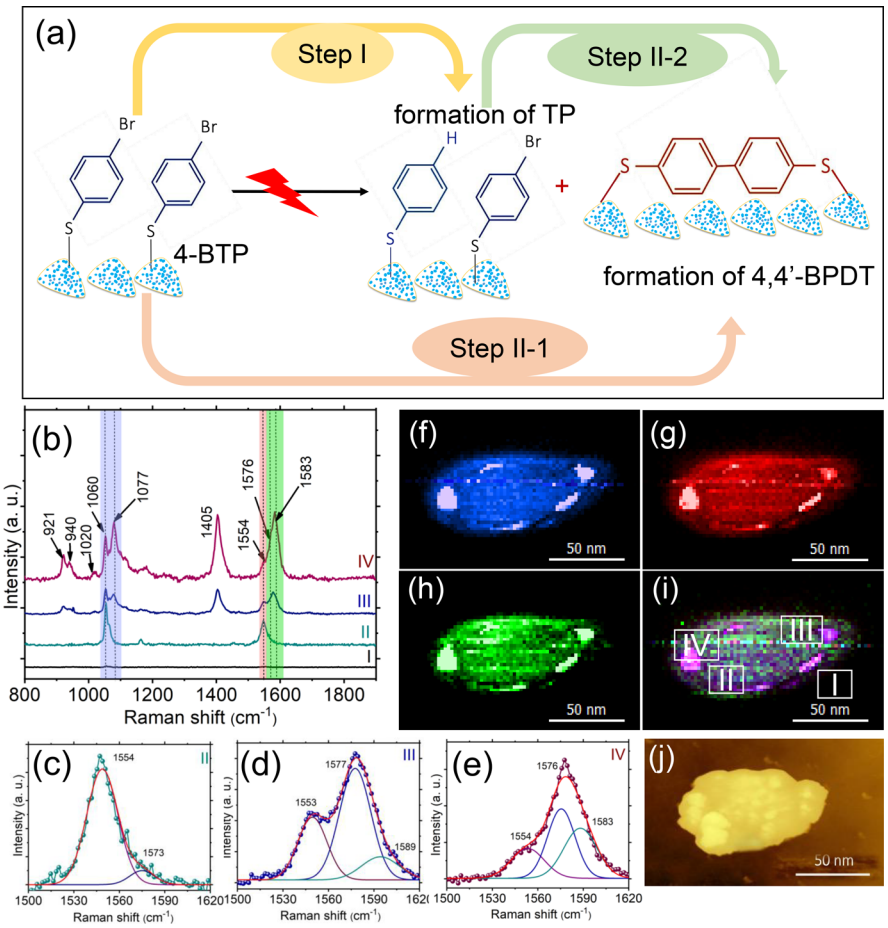

Figure 5. (a) Schematic representation of the catalytic reaction between 4-BTP to TP and 4,4′-BPDT on Au@NiNPs. Plasmon-driven formation of 4,4′-BPDT and TP on Au@NiNPs. (b) Selected TER spectra acquired from Au@NiNPs at different areas outlined in panel i. Deconvulated TER spectra in the region of 1500−1620 cm^{-1}, confirming the presence of intact 4-BTP (1554 cm^{-1} ($\nu C-C_{(ring)}$)) (c) and, in addition, the formation of TP (1575 cm^{-1} ($\nu C-C_{(ring)}$)) (d) and 4,4′-BPDT (1583 cm^{-1}) (e) on Au@NiNPs. TERS maps for the distributions of 4-BTP ((1060 cm^{-1} ($\nu C-Br$) and 1077 cm^{-1} (νCS)) (f), and 1554 cm^{-1} (g), TP (1575 cm^{-1}) and 4,4′-BPDT (1583 cm^{-1} (h)). (j) Overlay TERS map of panels f, g, and h. Reprinted with permission from ref 97. Copyright 2021 Royal Chemical Society.

excess of unbound 4-NBT.[65] Since the rate of the reaction was determined by covalently bound 4-NBT, the dimerization of 4-NBT on WS_2 nanoplates and WS_2@PdNPs hybrids was a pseudo-first-order reaction.

Monometallic and bimetallic TERS, as well as 2D TMDs, display distinct photocatalytic mechanisms due to differences in their electronic structures, charge transfer properties, and light−matter interactions. The photocatalytic reaction is primarily driven by plasmon-induced hot electron injection in metals, where LSPR excites carriers, leading to electron-driven catalysis.[105,106] 2D TMDs rely on bandgap excitation to generate e^-−h^+ pairs, which participate in oxidation−reduction reactions, with photogenerated excitons contributing to the catalytic processes. Additionally, in 2D TMDs, structural defects such as vacancies in dichalcogenides play a significant role in influencing photocatalytic activity.[107,108]

FUTURE PERSPECTIVES: NOVEL CHEMISTRY AND NOVEL MATERIALS

The reviewed studies highlighted the potential of TERS for nanoscale analysis of photocatalytic reactions on mono- and bimetallic nanostructures, as well as semiconductors. The strength of TERS lies not only in its nanoscale imaging capabilities but also in the quantitative aspects of the technique. With advances in technology and research, TERS holds exciting potential in key areas such as enhanced spatial resolution, in situ and real-time monitoring, nanoscale catalysis and reaction mechanisms, environmental and biochemical sensing, and material design and optimization, among others. Specifically, TERS can be used to determine the yield of chemical reactions as well as measure rates of catalytic reactions. Notably, this information can be obtained for individual surface sites, including corners, vacancies, adatoms, and flat terraces.[61−65,74,75,84,89,97,98,109,110] In turn, this information can be used to probe the mechanisms of catalytic reactions and reactivity of molecular analytes. For instance, Li and Kurouski examined molecular reactivity of aromatic halides in Suzuki−Miyaura coupling reaction using TERS.[110] It was found that 4-bromothiophenol was significantly more reactive compared with 4-chloro- and 4-fluorothiophenols.

Utilization of TERS, density functional theory (DFT) and time-dependent density functional theory (TDDFT) revealed molecular mechanisms of plasmon-driven reduction of nitro and carboxyl groups on AuNPs and Au@PdNPs.[111] It was found that a nitro group was far more reactive than a carboxyl group, which results in the formation of azo derivatives of 2-nitro-5-thiolobenzoic acid (2-N-5TBA) on AuNPs that later decarboxylate forming DMAB and then 4-NBT. On Au@PdNPs, 2-N-

https://doi.org/10.1021/acs.jpcc.5c01084
J. Phys. Chem. C 2025, 129, 7154−7164

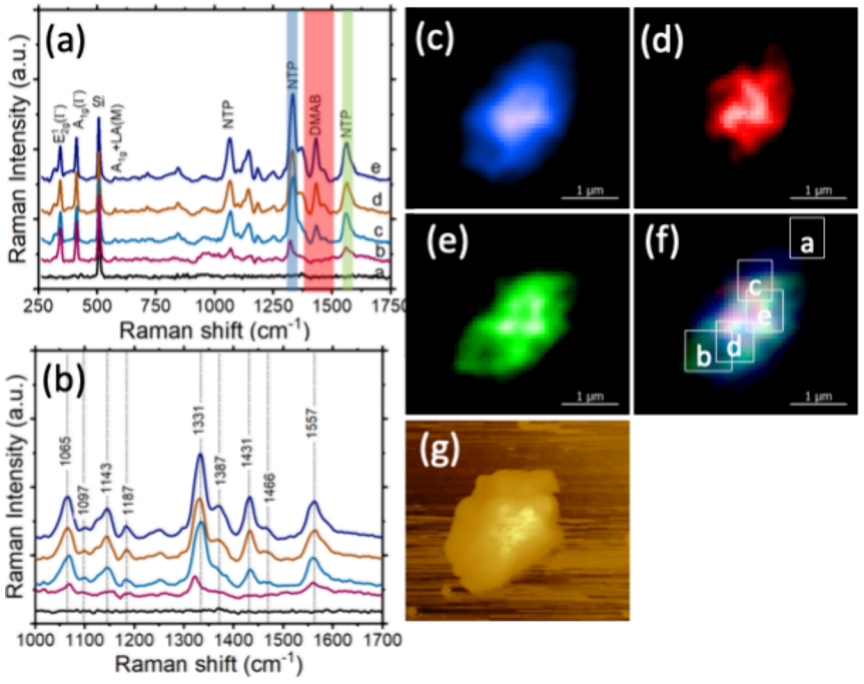

Figure 6. (a) Catalytic reactivity of the WS_2@PdNPs. (b) TER spectra extracted from chemical maps on 4-NTP decorated WS_2@PdNPs, showing the presence of 4-NTP and DMAB. (d–f) TERS images of WS_2: (c and e) 4-NTP and (d) DMAB; (f) overlapping 4-NTP and DMAB (intensity of 1331 and 1557 cm^{-1} band of 4-NTP, blue and green; intensity of 1387, 1431, and 1466 cm^{-1} band (azo vibration) of DMAB, red). (g) Corresponding AFM image of WS_2@PdNPs. The scanning step size was 10 nm per pixel, and the spectral acquisition time was 0.5 s. Reprinted with permission from ref 65. Copyright 2024 American Chemical Society.

5TBA first formed the bicarbonyl derivative of DMAB, which then was reduced to both bihydroxyl-DMAB and 4-amino-3-mercaptobenzoic acid.[111]

We also anticipate that TERS will be broadly used in the understanding of 2D and 3D materials physics. Recently, Gogotsi group used TERS to examine environmental stability of single-layer and few-layer flakes of $Ti_3C_2T_x$ MXene deposited on a gold substrate.[43] These and other studies demonstrate that TERS can be used for direct measurements of reactivity and structural properties of materials at the single-nanostructure level.[23,24,112,113] Jiang group demonstrated that a scanning probe could be used to trigger a dissociation of a specific molecular site (C–Si bond) in individual 5,10,15,20-(tetra(trimethylsilyl)-ethynyl)porphyrin molecules adsorbed on a Cu(100) surface.[114] To enable such bond scissoring, the scanning probe had to be positioned precisely at the chemical bond atop the molecule. Thus, TERS can be used to not only analyze the samples of interest but also alter their chemical structure.

It should be noted that with all of the above-discussed advantages, several inherent problems persist in TERS for years. One of them is the poor reliability of the scanning probes. Most research groups prepare their own scanning probes by simple thermal deposition of plasmonic metals[33,34,61,64,74,89,109,110,115] or electrochemical etching of Au or Ag wires.[23,24,112,113] Both of these methods do not allow for achieving the desired reproducibility and reliability of scanning probes. Spontaneous contamination of scanning probes is another issue broadly faced by all researchers that utilize TERS. It should be noted that contaminated scanning probes can be cleaned and reused.[116] Nevertheless, tip contamination enormously decelerates the nanoscale analysis of samples. Finally, the lifetime of the scanning probes remains short, ranging from minutes to days. Several engineering approaches were proposed to protect metallized scanning probes from both abrupt contamination and oxidation.[116] The Sokolov group proposed to coat Ag and Au probes with a few nanometers of aluminum (Al), which quickly turns into aluminum oxide that protects scanning probe from a mechanic deformation and oxidation.[117] Experimental validation of this strategy in our group showed a substantial decrease in the enhancement provided by such probes with only insignificant improvement in their lifetime. All of these limitations substantially decelerate the broad implication of TERS in biology and material science. Therefore, additional studies are needed to improve the robustness and reliability of the TERS.

Overall, the future of TERS in material science looks promising, as it holds the potential to provide unique insights into the properties, behaviors, and applications of materials at the nanoscale, driving innovations across various fields.

AUTHOR INFORMATION

Corresponding Author

Dmitry Kurouski – *Department of Biochemistry and Biophysics, Texas A&M University, College Station, Texas 77843, United States; Genetics Interdisciplinary Program, Texas A&M University, College Station, Texas 77843, United States;* orcid.org/0000-0002-6040-4213; Email: dkurouski@tamu.edu

Authors

Swati J. Patil – *Department of Biochemistry and Biophysics, Texas A&M University, College Station, Texas 77843, United States;* orcid.org/0000-0002-3619-2783

Charles L. Mitchell – *Department of Biochemistry and Biophysics, Texas A&M University, College Station, Texas 77843, United States; Genetics Interdisciplinary Program,*

https://doi.org/10.1021/acs.jpcc.5c01084
J. Phys. Chem. C 2025, 129, 7154–7164

Texas A&M University, College Station, Texas 77843, United States

Complete contact information is available at: https://pubs.acs.org/10.1021/acs.jpcc.5c01084

Notes

The authors declare no competing financial interest.

Biographies

Swati J. Patil earned her Ph.D. in Physics from Shivaji University in India. She began her career in 2016 as a postdoctoral researcher at Chonnam National University in South Korea, where she was promoted to research professor in 2017. Dr. Patil later became an Assistant Professor at Dongguk University, South Korea. In 2022, she joined the Kurouski Lab at Texas A&M University as an Assistant Research Scientist and is currently conducting research at the Texas A&M Research Center in Amarillo. Her research focuses on the development and optimization of advanced nanomaterials to tackle environmental challenges, improve energy systems, and promote environmental health.

Charles Mitchell earned his Bachelor of Science in Biochemistry from the University of Texas at Dallas and is a current graduate student in the Interdisciplinary Graduate Program in Genetics and Genomics at Texas A&M University. In 2023, he joined the Kurouski laboratory in the Biochemistry and Molecular Biophysics department. His research interests are centered around biological applications of transition metal dichalcogenide nanomaterials as potential therapeutics for neurological conditions.

Dr. Dmitry Kurouski received his M.Sc. in Biochemistry from Belarussian State University in 2007. After earning his Ph.D. in Analytical Chemistry from The State University of New York at Albany in 2013, Dr. Kurouski joined the Chemistry Department at Northwestern University where he worked as a postdoctoral fellow in the laboratory of Richard P. Van Duyne. Prior to Texas A&M University, Dr. Kurouski worked as a Senior Research Scientist at Boehringer-Ingelheim Pharmaceuticals. His research interests are focused on disease diagnostics in a large spectrum of biological species and elucidation of the underlying molecular causes of neurodegenerative diseases. His group pioneers the nanoscale analysis of photocatalytic processes using tip-enhanced Raman spectroscopy and atomic force microscopy Infrared spectroscopy.

■ ACKNOWLEDGMENTS

We are grateful to AgriLife Research of Texas A&M for the provided financial support. We also acknowledge Governor's University Research Initiative (GURI) grant program of Texas A&M University, GURI Grant Agreement No. 12-2016, M1700437. Abstract graphic was created with BioRender.com software.

■ REFERENCES

(1) Kleinman, S. L.; Frontiera, R. R.; Henry, A. I.; Dieringer, J. A.; Van Duyne, R. P. Creating, characterizing, and controlling chemistry with SERS hot spots. *Phys. Chem. Chem. Phys.* **2013**, *15* (1), 21−36.

(2) Brown, R. J.; Milton, M. J. T. Nanostructures and nanostructured substrates for surface-enhanced Raman scattering (SERS). *J. Raman. Spectr.* **2008**, *39*, 1313−1326.

(3) Moskovits, M. Surface roughness and the enhanced intensity of Raman scattering by molecules adsorbed on metals. *J. Chem. Phys.* **1978**, *69*, 4159−4161.

(4) Gersten, J.; Nitzan, A. Electromagnetic Theory of Enhanced Raman-Scattering by Molecules Adsorbed on Rough Surfaces. *J. Chem. Phys.* **1980**, *73*, 3023−3037.

(5) Kerker, M.; Wang, D. S.; Chew, H. Surface enhanced Raman scattering (SERS) by molecules adsorbed at spherical particles. *Applied optics* **1980**, *19* (19), 3373−3388.

(6) King, F. W.; Van Duyne, R. P.; Schatz, G. C. Theory of Raman scattering by molecules adsorbed on electrode surfaces. *J. Chem. Phys.* **1978**, *69* (10), 4472−4481.

(7) Sharma, B.; Frontiera, R. R.; Henry, A. I.; Ringe, E.; Van Duyne, R. P. SERS: Materials, applications, and the future. *Mater. Today* **2012**, *15* (1−2), 16−25.

(8) Kleinman, S. L.; Frontiera, R. R.; Henry, A. I.; Dieringer, J. A.; Van Duyne, R. P. Creating, characterizing, and controlling chemistry with SERS hot spots. *Phys. Chem. Chem. Phys.* **2013**, *15* (1), 21−36.

(9) Kurouski, D.; Lee, H.; Roschangar, F.; Senanayake, C. Surface-Enhanced Raman Spectroscopy: From Concept to Practical Application. *Spectroscopy* **2017**, *32*, 36−44.

(10) Stiles, P. L.; Dieringer, J. A.; Shah, N. C.; Van Duyne, R. P. Surface-enhanced Raman spectroscopy. *Annu. Rev. Anal Chem. (Palo Alto Calif)* **2008**, *1*, 601−626.

(11) Kelly, K. L.; Coronado, E.; Zhao, L. L.; Schatz, G. C. The Optical Properties of Metal Nanoparticles: The Influence of Size, Shape, and Dielectric Environment. *J. Phys. Chem. B* **2003**, *107* (3), 668−677.

(12) Wustholz, K. L.; Henry, A. I.; McMahon, J. M.; Freeman, R. G.; Valley, N.; Piotti, M. E.; Natan, M. J.; Schatz, G. C.; Van Duyne, R. P. Structure-activity relationships in gold nanoparticle dimers and trimers for surface-enhanced Raman spectroscopy. *J. Am. Chem. Soc.* **2010**, *132* (31), 10903−10910.

(13) Haes, A. J.; Haynes, C. L.; McFarland, A. D.; Schatz, G. C.; Van Duyne, R. P.; Zou, S. Plasmonic Materials for Surface-Enhanced Sensing and Spectroscopy. *MRS Bull.* **2005**, *30*, 368−375.

(14) Ringe, E.; McMahon, J. M.; Sohn, K.; Cobley, C.; Xia, Y.; Huang, J.; Schatz, G. C.; Marks, L. D.; Van Duyne, R. P. Unraveling the Effects of Size, Composition, and Substrate on the Localized Surface Plasmon Resonance Frequencies of Gold and Silver Nanocubes: A Systematic Single-Particle Approach. *J. Phys. Chem. C* **2010**, *114*, 12511−12516.

(15) Bingham, J. M.; Anker, J. N.; Kreno, L. E.; Van Duyne, R. P. Gas sensing with high-resolution localized surface plasmon resonance spectroscopy. *J. Am. Chem. Soc.* **2010**, *132* (49), 17358−17359.

(16) Kreno, L. E.; Hupp, J. T.; Van Duyne, R. P. Metal-organic framework thin film for enhanced localized surface plasmon resonance gas sensing. *Anal. Chem.* **2010**, *82* (19), 8042−8046.

(17) Lu, G.; Farha, O. K.; Kreno, L. E.; Schoenecker, P. M.; Walton, K. S.; Van Duyne, R. P.; Hupp, J. T. Fabrication of metal-organic framework-containing silica-colloidal crystals for vapor sensing. *Adv. Mater.* **2011**, *23* (38), 4449−4452.

(18) Kurouski, D.; Large, N.; Chiang, N.; Greeneltch, N.; Carron, K. T.; Seideman, T.; Schatz, G. C.; Van Duyne, R. P. Unraveling near-field and far-field relationships for 3D SERS substrates-a combined experimental and theoretical analysis. *Analyst* **2016**, *141* (5), 1779−1788.

(19) Henry, A. I.; Sharma, B.; Cardinal, M. F.; Kurouski, D.; Van Duyne, R. P. Surface-Enhanced Raman Spectroscopy Biosensing: In Vivo Diagnostics and Multimodal Imaging. *Anal. Chem.* **2016**, *88* (13), 6638−6647.

(20) Kleinman, S. L.; Frontiera, R. R.; Henry, A. I.; Dieringer, J. A.; Van Duyne, R. P. Creating, characterizing, and controlling chemistry with SERS hot spots. *Phys. Chem. Chem. Phys.* **2013**, *15* (1), 21−36.

(21) Sharma, B.; Frontiera, R. R.; Henry, A. I.; Ringe, E.; Van Duyne, R. P. SERS: Materials, applications, and the future. *Mater. Today* **2012**, *15* (1−2), 16−25.

(22) Jeanmaire, D. L.; Van Duyne, R. Surface raman spectroelectrochemistry: Part I. Heterocyclic, aromatic, and aliphatic amines adsorbed on the anodized silver electrode. *J. Electroanal. Chem. Interfac. Electrochem.* **1977**, *84*, 1−20.

(23) Jiang, N.; Foley, E. T.; Klingsporn, J. M.; Sonntag, M. D.; Valley, N. A.; Dieringer, J. A.; Seideman, T.; Schatz, G. C.; Hersam, M. C.; Van Duyne, R. P. Observation of multiple vibrational modes in ultrahigh vacuum tip-enhanced Raman spectroscopy combined with molecular-resolution scanning tunneling microscopy. *Nano Lett.* **2012**, *12* (10), 5061−5067.

(24) Klingsporn, J. M.; Jiang, N.; Pozzi, E. A.; Sonntag, M. D.; Chulhai, D.; Seideman, T.; Jensen, L.; Hersam, M. C.; Duyne, R. P. V. Intramolecular insight into adsorbate-substrate interactions via low-temperature, ultrahigh-vacuum tip-enhanced Raman spectroscopy. *J. Am. Chem. Soc.* **2014**, *136* (10), 3881−3887.
(25) Kurouski, D.; Mattei, M.; Van Duyne, R. P. Probing Redox Reactions at the Nanoscale with Electrochemical Tip-Enhanced Raman Spectroscopy. *Nano Lett.* **2015**, *15* (12), 7956−7962.
(26) Kurouski, D.; Zaleski, S.; Casadio, F.; Van Duyne, R. P.; Shah, N. C. Tip-enhanced Raman spectroscopy (TERS) for in situ identification of indigo and iron gall ink on paper. *J. Am. Chem. Soc.* **2014**, *136* (24), 8677−8684.
(27) Zhang, R.; Zhang, Y.; Dong, Z. C.; Jiang, S.; Zhang, C.; Chen, L. G.; Zhang, L.; Liao, Y.; Aizpurua, J.; Luo, Y.; et al. Chemical mapping of a single molecule by plasmon-enhanced Raman scattering. *Nature* **2013**, *498* (7452), 82−86.
(28) Lee, J.; Crampton, K. T.; Tallarida, N.; Apkarian, V. A. Visualizing vibrational normal modes of a single molecule with atomically confined light. *Nature* **2019**, *568* (7750), 78−82.
(29) Anderson, M. S. Locally Enchanced Raman Spectroscopy with an Atomic Force Microscope. *Appl. Phys. Lett.* **2000**, *76* (21), 3130−3132.
(30) Stöckle, R. M.; Suh, Y. D.; Deckert, V.; Zenobi, R. Nanoscale chemical analysis by tip-enhanced Raman spectroscopy. *Chem. Phys. Lett.* **2000**, *318* (1−3), 131−136.
(31) Hayazawa, N.; Inouye, Y.; Sekkat, Z.; Kawata, S. Metallized tip amplification of near-field Raman scattering. *Opt. Commun.* **2000**, *183* (1−4), 333−336.
(32) Böhme, R.; Mkandawire, M.; Krause-Buchholz, U.; Rösch, P.; Rödel, G.; Popp, J.; Deckert, V. Characterizing cytochrome c states - TERS studies of whole mitochondria. *Chem. Commun.* **2011**, *47* (41), 11453−11455.
(33) Kurouski, D.; Deckert-Gaudig, T.; Deckert, V.; Lednev, I. K. Structure and composition of insulin fibril surfaces probed by TERS. *J. Am. Chem. Soc.* **2012**, *134* (32), 13323−13329.
(34) Kurouski, D.; Deckert-Gaudig, T.; Deckert, V.; Lednev, I. K. Surface characterization of insulin protofilaments and fibril polymorphs using tip-enhanced Raman spectroscopy (TERS). *Biophys. J.* **2014**, *106* (1), 263−271.
(35) Lipiec, E.; Perez-Guaita, D.; Kaderli, J.; Wood, B. R.; Zenobi, R. Direct Nanospectroscopic Verification of the Amyloid Aggregation Pathway. *Angew. Chem., Int. Ed. Engl.* **2018**, *57*, 8519.
(36) Opilik, L.; Payamyar, P.; Szczerbiński, J.; Schütz, A. P.; Servalli, M.; Hungerland, T.; Schlüter, A. D.; Zenobi, R. Minimally Invasive Characterization of Covalent Monolayer Sheets Using Tip-Enhanced Raman Spectroscopy. *ACS Nano* **2015**, *9* (4), 4252−4259.
(37) Cai, Z. F.; Merino, J. P.; Fang, W.; Kumar, N.; Richardson, J. O.; De Feyter, S.; Zenobi, R. Molecular-Level Insights on Reactive Arrangement in On-Surface Photocatalytic Coupling Reactions Using Tip-Enhanced Raman Spectroscopy. *J. Am. Chem. Soc.* **2022**, *144* (1), 538−546.
(38) Dai, W.; Shao, F.; Szczerbiński, J.; McCaffrey, R.; Zenobi, R.; Jin, Y.; Schlüter, A. D.; Zhang, W. Synthesis of a Two-Dimensional Covalent Organic Monolayer through Dynamic Imine Chemistry at the Air/Water Interface. *Angew. Chem., Int. Ed. Engl.* **2016**, *128* (1), 221−225.
(39) Zeng, Z. C.; Huang, S. C.; Wu, D. Y.; Meng, L. Y.; Li, M. H.; Huang, T. X.; Zhong, J. H.; Wang, X.; Yang, Z. L.; Ren, B. Electrochemical Tip-Enhanced Raman Spectroscopy. *J. Am. Chem. Soc.* **2015**, *137* (37), 11928−11931.
(40) Martin Sabanes, N.; Ohto, T.; Andrienko, D.; Nagata, Y.; Domke, K. F. Electrochemical TERS Elucidates Potential-Induced Molecular Reorientation of Adenine/Au(111). *Angew. Chem., Int. Ed. Engl.* **2017**, *56* (33), 9796−9801.
(41) Pfisterer, J. H. K.; Baghernejad, M.; Giuzio, G.; Domke, K. F. Reactivity mapping of nanoscale defect chemistry under electrochemical reaction conditions. *Nat. Commun.* **2019**, *10* (1), 5702.
(42) Yin, H.; Zheng, L. Q.; Fang, W.; Lai, Y.-H.; Porenta, N.; Goubert, G.; Zhang, H.; Su, H. S.; Ren, B.; Richardson, J. O.; et al. Nanometre-scale spectroscopic visualization of catalytic sites during a hydrogenation reaction on a Pd/Au bimetallic catalyst. *Nat. Energy.* **2020**, *3*, 834−842.
(43) Sarycheva, A.; Shanmugasundaram, M.; Krayev, A.; Gogotsi, Y. Tip-Enhanced Raman Scattering Imaging of Single- to Few-Layer Ti3C2Tx MXene. *ACS Nano* **2022**, *16*, 6858.
(44) Su, W.; Kumar, N.; Krayev, A.; Chaigneau, M. In situ topographical chemical and electrical imaging of carboxyl graphene oxide at the nanoscale. *Nat. Commun.* **2018**, *9* (1), 2891.
(45) Wang, C. F.; O'Callahan, B. T.; Kurouski, D.; Krayev, A.; El-Khoury, P. Z. The Prevalence of Anions at Plasmonic Nanojunctions: A Closer Look at p-Nitrothiophenol. *J. Phys. Chem. Lett.* **2020**, *11* (10), 3809−3814.
(46) Zhang, Z. L.; Xu, P.; Yang, X. Z.; Liang, W. J.; Sun, M. T. Surface plasmon-driven photocatalysis in ambient, aqueous and high-vacuum monitored by SERS and TERS. *J. Photoch Photobio C* **2016**, *27*, 100−112.
(47) Li, Z. D.; Kurouski, D. Nanoscale structural characterization of plasmon-driven reactions. *Nanophotonics-Berlin* **2021**, *10* (6), 1657−1673.
(48) Li, Z. D.; Kurouski, D. Plasmon-Driven Chemistry on Mono- and Bimetallic Nanostructures. *Acc. Chem. Res.* **2021**, *54* (10), 2477−2487.
(49) Khurgin, J. B. How to deal with the loss in plasmonics and metamaterials. *Nat. Nanotechnol.* **2015**, *10* (1), 2−6.
(50) Narang, P.; Sundararaman, R.; Atwater, H. A. Plasmonic hot carrier dynamics in solid-state and chemical systems for energy conversion. *Nanophotonics* **2016**, *5* (1), 96−111.
(51) Manjavacas, A.; Liu, J. G.; Kulkarni, V.; Nordlander, P. Plasmon-induced hot carriers in metallic nanoparticles. *ACS Nano* **2014**, *8* (8), 7630−7638.
(52) Brown, A. M.; Sundararaman, R.; Narang, P.; Goddard, W. A., III; Atwater, H. A. Nonradiative plasmon decay and hot carrier dynamics: effects of phonons, surfaces, and geometry. *ACS Nano* **2016**, *10* (1), 957−966.
(53) Hartland, G. V. Optical studies of dynamics in noble metal nanostructures. *Chem. Rev.* **2011**, *111* (6), 3858−3887.
(54) Ma, J.; Wang, Z.; Wang, L.-W. Interplay between plasmon and single-particle excitations in a metal nanocluster. *Nat. Commun.* **2015**, *6*, 10107.
(55) Cortés, E.; Xie, W.; Cambiasso, J.; Jermyn, A. S.; Sundararaman, R.; Narang, P.; Schlücker, S.; Maier, S. A. Plasmonic hot electron transport drives nano-localized chemistry. *Nat. Commun.* **2017**, *8*, 14880.
(56) Redmond, P. L.; Brus, L. E. "Hot Electron" Photo-Charging and Electrochemical Discharge Kinetics of Silver Nanocrystals. *J. Phys. Chem. C* **2007**, *111*, 14849−11485.
(57) Wilson, A. J.; Jain, P. K. Light-Induced Voltages in Catalysis by Plasmonic Nanostructures. *Acc. Chem. Res.* **2020**, *53*, 1773−1781.
(58) Yu, S.; Jain, P. K. The Chemical Potential of Plasmonic Excitations. *Angew. Chem., Int. Ed.* **2020**, *59*, 2085−2088.
(59) Yu, S.; Wilson, A. J.; Heo, J.; Jain, P. K. Plasmonic Control of Multi-Electron Transfer and C-C Coupling in Visible-Light-Driven CO2 Reduction on Au Nanoparticles. *Nano Lett.* **2018**, *18*, 2189−2194.
(60) Yu, S.; Jain, P. K. The Chemical Potential of Plasmonic Excitations. *Angew. Chem., Int. Ed. Engl.* **2020**, *59* (5), 2085−2088.
(61) Li, Z.; Kurouski, D. Plasmon-Driven Chemistry on Mono- and Bimetallic Nanostructures. *Acc. Chem. Res.* **2021**, *54* (10), 2477−2487.
(62) Li, Z.; Rigor, J.; Large, N.; El-Khoury, P.; Kurouski, D. Underlying Mechanisms of Hot Carrier-Driven Reactivity on Bimetallic Nanostructures. *J. Phys. Chem. C* **2021**, *125*, 2492−2501.
(63) Li, Z.; Kurouski, D. Can Light Alter the Yield of Plasmon-Driven Reactions on Gold and Gold-Palladium Nanoplates? *Nano Lett.* **2022**, *22* (18), 7484−7491.
(64) Li, Z.; Kurouski, D. Probing the Redox Selectivity on Au@Pd and Au@Pt Bimetallic Nanoplates by Tip-Enhanced Raman Spectroscopy. *ACS Photonics* **2021**, *8* (7), 2112−2119.
(65) Patil, S. J.; Kurouski, D. Nanoscale Imaging of Palladium-Enhanced Photocatalytic Reduction of 4-Nitrothiophenol on Tungsten Disulfide Nanoplates. *Nano Lett.* **2024**, *24* (41), 13004−13009.

https://doi.org/10.1021/acs.jpcc.5c01084
J. Phys. Chem. C 2025, 129, 7154−7164

(66) Singh, K. A.; Soukar, J.; Zulkifli, M.; Kersey, A.; Lokhande, G.; Ghosh, S.; Murali, A.; Garza, N. M.; Kaur, H.; Keeney, J. N.; et al. Atomic vacancies of molybdenum disulfide nanoparticles stimulate mitochondrial biogenesis. *Nat. Commun.* **2024**, *15* (1), 8136.
(67) Park, K. D.; Jiang, T.; Clark, G.; Xu, X.; Raschke, M. B. Radiative control of dark excitons at room temperature by nano-optical antenna-tip Purcell effect. *Nat. Nanotechnol* **2018**, *13* (1), 59−64.
(68) Park, K. D.; Khatib, O.; Kravtsov, V.; Clark, G.; Xu, X.; Raschke, M. B. Hybrid Tip-Enhanced Nanospectroscopy and Nanoimaging of Monolayer WSe2 with Local Strain Control. *Nano Lett.* **2016**, *16* (4), 2621−2627.
(69) Park, K. D.; Muller, E. A.; Kravtsov, V.; Sass, P. M.; Dreyer, J.; Atkin, J. M.; Raschke, M. B. Variable-Temperature Tip-Enhanced Raman Spectroscopy of Single-Molecule Fluctuations and Dynamics. *Nano Lett.* **2016**, *16* (1), 479−487.
(70) Luo, W. J.; Song, R. K.; Whetten, B. G.; Huang, D.; Cheng, X. B.; Belyanin, A.; Jiang, T.; Raschke, M. B. Nonlinear Nano-Imaging of Interlayer Coupling in 2D Graphene-Semiconductor Heterostructures. *Small* **2024**, *20* (24), 2307345.
(71) Hasz, K.; Hu, Z.; Park, K. D.; Raschke, M. B. Tip-Enhanced Dark Exciton Nanoimaging and Local Strain Control in Monolayer WSe2. *Nano Lett.* **2023**, *23* (1), 198−204.
(72) Wang, G. C.; Li, L.; Fan, W. H.; Wang, R. Y.; Zhou, S. S.; Lue, J. T.; Gan, L.; Zhai, T. Y. Interlayer Coupling Induced Infrared Response in WS/MoS Heterostructures Enhanced by Surface Plasmon Resonance. *Adv. Funct Mater.* **2018**, *28* (22), 1800339.
(73) van Schrojenstein Lantman, E. M.; Deckert-Gaudig, T.; Mank, A. J.; Deckert, V.; Weckhuysen, B. M. Catalytic processes monitored at the nanoscale with tip-enhanced Raman spectroscopy. *Nat. Nanotechnol.* **2012**, *7* (9), 583−586.
(74) Li, Z.; Kurouski, D. Elucidation of Photo-Catalytic Properties of Goldplatinum Bimetallic Nanoplates Using Tip-Enhanced Raman Spectroscopy. *J. Phys. Chem. C* **2020**, *124*, 12850−12854.
(75) Li, Z.; Wang, R.; Kurouski, D. Nanoscale Photocatalytic Activity of Gold and Gold-Palladium Nanostructures Revealed by Tip-Enhanced Raman Spectroscopy. *J. Phys. Chem. Lett.* **2020**, *11*, 5531−5537.
(76) Li, Z.; El-Khoury, P.; Kurouski, D. Tip-Enhanced Raman Imaging of Photocatalytic Reactions on Thermally-Reshaped Gold and Gold-Palladium Microplates. *Chem. Commun.* **2021**, *57*, 891.
(77) Marr, J. M.; Schultz, Z. D. Imaging Electric Fields in SERS and TERS Using the Vibrational Stark Effect. *J. Phys. Chem. Lett.* **2013**, *4* (19), 3268.
(78) Kwasnieski, D. T.; Wang, H.; Schultz, Z. D. Alkyl-Nitrile Adlayers as Probes of Plasmonically Induced Electric Fields. *Chem. Sci.* **2015**, *6* (8), 4484−4494.
(79) Nelson, D. A.; Schultz, Z. D. Influence of Optically Rectified Electric Fields on the Plasmonic Photocatalysis of 4-Nitrothiophenol and 4-Aminothiophenol to 4,4-Dimercaptoazobenzene. *J. Phys. Chem. C* **2018**, *122*, 8581−8588.
(80) Bhattarai, A.; Crampton, K. T.; Joly, A. G.; Kovarik, L.; Hess, W. P.; El-Khoury, P. Z. Imaging the Optical Fields of Functionalized Silver Nanowires through Molecular TERS. *J. Phys. Chem. Lett.* **2018**, *9* (24), 7105−7109.
(81) Bhattarai, A.; Novikova, I. V.; El-Khoury, P. Z. Tip-Enhanced Raman Nanographs of Plasmonic Silver Nanoparticles. *J. Phys. Chem. C* **2019**, *123*, 27765−27769.
(82) Mayevsky, A. D.; Funston, A. M. Control of Electric Field Localization by Three-Dimensional Bowtie Nanoantennae. *J. Phys. Chem. C* **2018**, *122*, 18012−18020.
(83) Yang, H.; Owiti, E. O.; Jiang, X.; Li, S.; Liu, P.; Sun, X. Localized Surface Plasmon Resonance Dependence on Misaligned Truncated Ag Nanoprism Dimer. *Nanoscale Res. Lett.* **2017**, *12* (1), 430.
(84) Li, Z.; Rigor, J.; Ehtesabi, S.; Gojare, S.; Kupfer, S.; Grafe, S.; Large, N.; Kurouski, D. Role of Plasmonic Antenna in Hot Carrier-Driven Reactions on Bimetallic Nanostructures. *J. Phys. Chem. C* **2023**, *127* (46), 22635−22645.
(85) Sun, J.-J.; Su, H.-S.; Yue, H.-L.; Huang, S.-C.; Huang, T.-X.; Hu, S.; Sartin, M. M.; Cheng, J.; Ren, B. Role of adsorption orientation in surface plasmon-driven coupling reactions studied by tip-enhanced Raman spectroscopy. *J. Phys. Chem. Lett.* **2019**, *10* (10), 2306−2312.
(86) Wang, R.; Kurouski, D. Thermal Reshaping of Gold Microplates: Three Possible Routes and Their Transformation Mechanisms. *ACS Appl. Mater. Interfaces* **2019**, *11* (44), 41813−41820.
(87) Wang, R.; Kurouski, D. Elucidation of Tip-Broadening Effect in Tip-Enhanced Raman Spectroscopy (TERS): A Cause of Artifacts or Potential for 3D TERS. *J. Phys. Chem. C* **2018**, *122*, 24334−24340.
(88) Rossi, T. P.; Erhart, P.; Kuisma, M. Hot-Carrier Generation in Plasmonic Nanoparticles: The Importance of Atomic Structure. *ACS Nano* **2020**, *14* (8), 9963−9971.
(89) Li, Z.; Kurouski, D. Tip-Enhanced Raman Analysis of Plasmonic and Photocatalytic Properties of Copper Nanomaterials. *J. Phys. Chem. Lett.* **2021**, *12* (34), 8335−8340.
(90) Patil, S. J.; Lomonosov, V.; Ringe, E.; Kurouski, D. Tip-Enhanced Raman Imaging of Plasmon-Driven Coupling of 4-Nitrobenzenethiol on Au-Decorated Magnesium Nanostructures. *J. Phys. Chem. C Nanomater Interfaces* **2023**, *127* (16), 7702−7706.
(91) Sytwu, K.; Vadai, M.; Dionne, J. A. Bimetallic nanostructures: combining plasmonic and catalytic metals for photocatalysis. *Advances in Physics: X* **2019**, *4* (1), 1619480.
(92) Brongersma, M. L.; Halas, N. J.; Nordlander, P. Plasmon-induced hot carrier science and technology. *Nat. Nanotechnol.* **2015**, *10* (1), 25−34.
(93) Zhou, L.; Martirez, J. M. P.; Finzel, J.; Zhang, C.; Swearer, D. F.; Tian, S.; Robatjazi, H.; Lou, M.; Dong, L.; Henderson, L.; et al. Light-driven methane dry reforming with single atomic site antenna-reactor plasmonic photocatalysts. *Nature Energy* **2020**, *5*, 61−70.
(94) Zhong, J. H.; Jin, X.; Meng, L.; Wang, X.; Su, H. S.; Yang, Z. L.; Williams, C. T.; Ren, B. Probing the electronic and catalytic properties of a bimetallic surface with 3 nm resolution. *Nature Nanotechnol.* **2017**, *12* (2), 132−136.
(95) Su, H. S.; Zhang, X. G.; Sun, J. J.; Jin, X.; Wu, D. Y.; Lian, X. B.; Zhong, J. H.; Ren, B. Real-Space Observation of Atomic Site-Specific Electronic Properties of a Pt Nanoisland/Au(111) Bimetallic Surface by Tip-Enhanced Raman Spectroscopy. *Angew. Chem., Int. Ed. Engl.* **2018**, *57* (40), 13177−13181.
(96) Yin, H.; Zheng, L.; Fang, W.; Lai, H. L.; Porenta, N.; Goubert, G.; Zhang, H.; Su, H. S.; Ren, B.; Richardson, J. O.; et al. Nanometre- scale spectroscopic visualization of catalytic sites during a hydrogenation reaction on a Pd/Au bimetallic catalyst. *Nat. Catal.* **2020**, *3*, 834−842.
(97) Patil, S. J.; Kurouski, D. Tip-enhanced Raman imaging of plasmon-driven dimerization of 4-bromothiophenol on nickel-decorated gold nanoplate bimetallic nanostructures. *Chem. Commun. (Camb)* **2023**, *59* (73), 10976−10979.
(98) Patil, S. J.; Kurouski, D. Chemical Nanoimaging and Characterizing Kinetics of Bimetallic Nanostructure-Plasmon-Driven Dimerization Reactions by TipEnhanced Raman Spectroscopy. *J. Phys. Chem. C* **2024**, *128*, 242−247.
(99) Yang, R. J.; Fan, Y. Y.; Zhang, Y. F.; Mei, L.; Zhu, R. S.; Qin, J. Q.; Hu, J. G.; Chen, Z. X.; Ng, Y. H.; Voiry, D. 2D Transition Metal Dichalcogenides for Photocatalysis. *Angew. Chem. Int. Ed* **2023**, *62* (13), e202218016.
(100) Velicky, M.; Rodriguez, A.; Bousa, M.; Krayev, A. V.; Vondrácek, M.; Honolka, J.; Ahmadi, M.; Donnelly, G. E.; Huang, F. M.; Abruña, H. D.; et al. Strain and Charge Doping Fingerprints of the Strong Interaction between Monolayer MoS and Gold. *J. Phys. Chem. Lett.* **2020**, *11* (15), 6112−6118.
(101) Lambin, C.; Avilés, M. O.; Jelken, J.; Lagugné-Labarthet, F. Molybdenum Disulfide Flakes as Platforms for the Photoconversion of 4-Nitrothiophenol. *J. Phys. Chem. C* **2023**, *127* (50), 24281−24290.
(102) Rizevsky, S.; Kurouski, D. Tip-Enhanced Raman Imaging of Photocatalytic Processes at the Nanoscale. *J. Phys. Chem. C* **2022**, *126* (35), 14781−14790.
(103) Lambin, C.; Mccarvell, W. M.; Cheng, P. S.; Lau-Truong, S.; Decorse, P.; Mangeney, C.; Félidj, N.; Lagugné-Labarthet, F. Tuning the Band Gap of MoS Single Layer with Aryl Diazonium Salts. *J. Phys. Chem. C* **2025**, *129* (10), 5105−5115.

https://doi.org/10.1021/acs.jpcc.5c01084
J. Phys. Chem. C 2025, 129, 7154−7164

(104) Farhat, P.; Avilés, M. O.; Legge, S.; Wang, Z. Q.; Sham, T. K.; Lagugné-Labarthet, F. Tip-Enhanced Raman Spectroscopy and Tip-Enhanced Photoluminescence of MoS Flakes Decorated with Gold Nanoparticles. *J. Phys. Chem. C* **2022**, *126* (16), 7086−7095.
(105) Zhou, L.; Huang, Q. J.; Xia, Y. N. Plasmon-Induced Hot Electrons in Nanostructured Materials: Generation, Collection, and Application to Photochemistry. *Chem. Rev.* **2024**, *124* (14), 8597−8619.
(106) Sobhani, A.; Knight, M. W.; Wang, Y. M.; Zheng, B.; King, N. S.; Brown, L. V.; Fang, Z. Y.; Nordlander, P.; Halas, N. J. Narrowband photodetection in the near-infrared with a plasmon-induced hot electron device. *Nat. Commun.* **2013**, *4*, 1643.
(107) Zavabeti, A.; Jannat, A.; Zhong, L.; Haidry, A. A.; Yao, Z. J.; Ou, J. Z. Two-Dimensional Materials in Large-Areas: Synthesis, Properties and Applications. *Nano-Micro Lett.* **2020**, *12* (1), 66.
(108) Liang, Q. J.; Zhang, Q.; Zhao, X. X.; Liu, M. Z.; Wee, A. T. S. Defect Engineering of Two-Dimensional Transition-Metal Dichalcogenides: Applications, Challenges, and Opportunities. *ACS Nano* **2021**, *15* (2), 2165−2181.
(109) Li, Z.; Kurouski, D. Nanoscale structural characterization of plasmon-driven reactions. *Nanophotonics* **2021**, *10*, 1657−1673.
(110) Li, Z.; Kurouski, D. Probing the plasmon-driven Suzuki-Miyaura coupling reactions with cargo-TERS towards tailored catalysis. *Nanoscale* **2021**, *13* (27), 11793−11799.
(111) Li, Z.; Ehtesabi, S.; Gojare, S.; Richter, M.; Kupfer, S.; Grafe, S.; Kurouski, D. Plasmon-Determined Selectivity in Photocatalytic Transformations on Gold and Gold-Palladium Nanostructures. *ACS Photonics* **2023**, *10* (9), 3390−3400.
(112) Mahapatra, S.; Ning, Y.; Schultz, J. F.; Li, L.; Zhang, J. L.; Jiang, N. Angstrom Scale Chemical Analysis of Metal Supported Trans- and Cis-Regioisomers by Ultrahigh Vacuum Tip-Enhanced Raman Mapping. *Nano Lett.* **2019**, *19* (5), 3267−3272.
(113) Chiang, N.; Chen, X.; Goubert, G.; Chulhai, D. V.; Chen, X.; Pozzi, E. A.; Jiang, N.; Hersam, M. C.; Seideman, T.; Jensen, L.; et al. Conformational Contrast of Surface-Mediated Molecular Switches Yields Angstrom-Scale Spatial Resolution in Ultrahigh Vacuum Tip-Enhanced Raman Spectroscopy. *Nano Lett.* **2016**, *16* (12), 7774−7778.
(114) Mahapatra, S.; Schultz, J. F.; Li, L.; Zhang, X.; Jiang, N. Controlling Localized Plasmons via an Atomistic Approach: Attainment of Site-Selective Activation inside a Single Molecule. *J. Am. Chem. Soc.* **2022**, *144* (5), 2051−2055.
(115) Richard-Lacroix, M.; Deckert, V. Direct molecular-level near-field plasmon and temperature assessment in a single plasmonic hotspot. *Light Sci. Appl.* **2020**, *9*, 35.
(116) Huang, T. X.; Huang, S. C.; Li, M. H.; Zeng, Z. C.; Wang, X.; Ren, B. Tip-enhanced Raman spectroscopy: tip-related issues. *Anal Bioanal Chem.* **2015**, *407* (27), 8177−8195.
(117) Agapov, R. L.; Sokolov, A. P.; Foster, M. D. Protecting TERS probes from degradation: extending mechanical and chemical stability. *J. Raman Spectrosc.* **2013**, *44* (5), 710−716.

https://doi.org/10.1021/acs.jpcc.5c01084
J. Phys. Chem. C 2025, 129, 7154−7164